One-component plasma of point charges and of charged rods

Marius M. Hatlo, Argyrios Karatrantos, and Leo Lue*
School of Chemical Engineering and Analytical Science, The University of Manchester, P.O. Box 88, Sackville Street, Manchester M60 1QD, United Kingdom

(Received 30 March 2009; revised manuscript received 3 September 2009; published 8 December 2009)

An approximate theory is developed to describe the properties of mobile particles with extended charge distributions in the presence of a neutralizing fixed background charge. Long-wavelength fluctuations of the electric potential are handled within a variational perturbation approximation, and the short-wavelength fluctuations are handled within a cumulant (fugacity) expansion. The distinct treatment of these two contributions to the free energy enables the theory to provide quantitative predictions for the properties of these systems from the weak- to the strong-coupling regimes. With this theory, we study three different variations in the classical one-component plasma model: a plasma of point charges, a plasma of particles consisting of 8 linearly bonded point charges (8-mer), and a plasma of line charges. The theory was found to agree well with the available computer simulation data for the electrostatic interaction energy of these systems for all values of the plasma coupling parameter examined ($\Gamma=0$ to 400). In addition, we find that both the 8-mer rod and the line charge systems form a strongly ordered nematic phase, which is entirely driven by electrostatic interactions. The nematic phase only exists within a finite range of lengths of the charged particles. If the particles are too short or too long, the nematic phase does not appear. Finally, we find that the nematic phase is stable over a broader range of conditions for the line charge system than for the 8-mer rod system; consequently, the phase behavior of the one-component plasma is sensitive to the manner in which the charge is distributed on the particles.

DOI: 10.1103/PhysRevE.80.061107 PACS number(s): 05.20.Jj, 52.25.Kn, 05.70.Ce, 61.30.Cz

I. INTRODUCTION

Electrostatic interactions play a significant role in determining the properties of many soft matter systems; consequently, they have received a lot of attention over the last hundred years. One of the simplest systems that possesses electrostatic interactions is the classical one-component plasma (OCP) [1,2], which consists of mobile point charges in a rigid neutralizing background charge. In addition to providing a starting point to test theories, the classical OCP is also a good physical model for important systems, such as the interior of massive planets and the classical electron gas. Much of the theoretical work on this system has been based on integral equation approaches, such as the mean spherical approximation [3,4], the hypernetted-chain (HNC) approximation [5,6], the reference HNC approximation [7], and the hybrid HNC and Percus-Yevick closures [8]. These theories provide accurate descriptions for both the structure and thermodynamic properties in comparison to computer simulation data; however, due to their complexity, computational expense, and lack of a physical motivation for the approximate closure relations, the development of other simpler methods have been pursued to model the OCP. Examples include the correlation hole corrected Debye-Hückel theory [9] and field theory approaches with a high wave-vector cutoff [10,11]. These simpler approaches can also describe the computer simulation data, which indicates that they capture the essential physics. However, the downside of these approaches is the need to include an empirical parameter, based on physical grounds, such as the size of the correlation hole [9,12] or the magnitude of a high wave-vector cutoff [10,11].

Related to the OCP are systems of counterions near charged surfaces, which has been extensively studied with both theory and computer simulation. These systems can be viewed as a one-component plasma, but with the background charge concentrated on surfaces rather than uniformly distributed in space. When the electrostatic interactions are weak, these systems are well described by the Poisson-Boltzmann theory; however, this theory breaks down at high surface charge densities and cannot describe the attractive interactions that occur between similarly charged surfaces at these conditions [13]. Corrections to the Poisson-Boltzmann theory can be obtained systematically through a loop expansion; unfortunately, high-order calculations, which become increasingly complex, are required to obtain accurate results when the electrostatic interactions become significant. In the limit of extremely high electrostatic couplings, a strong-coupling expansion [14,15] has been successfully developed. This is essentially an expansion in the fugacity of the counterions. The region of intermediate electrostatic couplings is, however, problematic. One approach to describe these conditions relies on the use of test charges; this includes the modified Poisson-Boltzmann theory [16–18] and the work of Burak *et al.* [19].

One fruitful approach for dealing with the difficult nature of these systems at all electrostatic couplings is to divide the Coulomb interactions into short-wavelength and long-wavelength contributions [20–23] and to treat each of these within a separate approximation scheme. The short-wavelength fluctuations of the electric potential, which are due to highly interacting counterions, are well approximated within the strong-coupling expansion; the long-wavelength fluctuations are weak and are well approximated by a mean-field or loop expansion. This approach leads to a theory [23], which is capable of quantitatively predicting the properties of the charged plate/counterion system from the weak- to the

*leo.lue@manchester.ac.uk

strong-coupling regimes, even in the presence of dielectric inhomogeneities. One major advantage of this theory is that it has a similar computational complexity to the original Poisson-Boltzmann theory.

A simple extension of the OCP model is to replace the point charges with particles that have an extended charge distribution. One example is a system of line charges, which serves as a simple model of linear polyelectrolyte solutions. Within this model, the counterions that are present in real polyelectrolyte solutions are represented by the rigid neutralizing background charge. Because of their significance in many practical applications and their interesting behavior, there are a tremendous number of theoretical studies of polyelectrolyte solutions, and we refer the readers to the review articles [24–26]. In this work, however, we limit ourselves to the OCP model, which can be considered as providing a description of polyelectrolyte solutions that is complementary to the cell model [27–33]. In the cell model, the counterions are explicitly considered; however, the correlations between the polyelectrolytes are only indirectly accounted for. In the case of the OCP, the correlations between the polyelectrolytes are explicitly considered; however, the counterions are only considered as a uniform background charge.

Deutsch and Goldenfeld studied [34,35] the OCP of line charges with a theory based on an extension of the Debye-Hückel theory and found that it exhibited a strong first-order isotropic to nematic ordering of the lines. Integral equation theories [26,36,37] have also been used to describe systems of rodlike polyelectrolytes. Typically, these approaches work well for low electrostatic coupling and polyelectrolyte densities but only qualitatively at high electrostatic coupling and high densities. Carri and Muthukumar [38] developed theories for linear rod polyelectrolytes, with an effective pair potential to represent a screened Coulomb interaction, to calculate the thermodynamic behavior of semidilute solutions. A loop expansion approach was taken by Potemkin and Khokhlov [39–41] to study the nematic ordering of rodlike polyelectrolytes in dilute solutions. Due to the nature of the approximations made, these theories are typically limited to relatively weakly charged polyelectrolytes.

In this work, we develop a simple field-theoretic approach for the one-component plasma model. By treating the short- and long-wavelength fluctuations of the electric potential within separate approximations, the theory can successfully describe the OCP over a broad range of coupling parameters. This work is an extension of previous work [23] for point-charge systems to particles with extended charge distributions. The remainder of this paper is organized as follows. In Sec. II, we develop a field-theoretic approach to describing charged particles. This approach divides the short- and long-wavelength phenomena and treats them within different approximations. Consequently, it is able to accurately describe the properties of charge systems, even when they are strongly coupled. In Sec. III, we then apply this theory to the classical OCP of point charges, comparing the results with available simulation data. In Sec. IV, we proceed to examine a system, where the point charges are rigidly bonded into a linear rod. The theoretical predictions are compared against molecular-dynamics simulations. We then study a one-component plasma of line charges in Sec. V. In Sec. VI, we analyze the possibility of formation of an orientationally ordered nematic phase by the charged rod systems. We find that under certain conditions, these systems possess a strong isotropic to nematic transition driven purely by the electrostatics. Finally, the main findings of this paper are summarized in Sec. VII.

II. THEORY

In this work, we consider a one-component plasma of identical particles in a fixed neutralizing background charge density $\Sigma(\mathbf{r})$ and a dielectric constant ϵ. Each of the particles has a rigid charge distribution with a total charge q. The charge density $Q(\mathbf{r},\mathbf{\Omega})$ due to a particle located at the origin and in orientation $\mathbf{\Omega}$ is given by

$$Q(\mathbf{r},\mathbf{\Omega}) = \int ds q(s) \delta^3[\mathbf{r} - \mathbf{A}(\mathbf{\Omega}) \cdot \delta\mathbf{R}(s)], \tag{1}$$

where $\delta\mathbf{R}(s)$ is the position of segment s of the particle relative to some reference orientation and position within the molecule, $q(s)$ is the charge of segment s of the particle, and $\mathbf{A}(\mathbf{\Omega})$ is a rotation matrix, which transforms the particle from its reference orientation to the orientation $\mathbf{\Omega}$.

The charge density $q(\mathbf{r})$ of mobile particles is given by

$$q(\mathbf{r}) = \sum_k Q(\mathbf{r} - \mathbf{R}_k, \mathbf{\Omega}_k). \tag{2}$$

The total charge density $\mathcal{Q}(\mathbf{r})$ in the system is given by the sum of the contributions from the mobile particles and the fixed background charge

$$\mathcal{Q}(\mathbf{r}) = q(\mathbf{r}) + \Sigma(\mathbf{r}) = \sum_k Q(\mathbf{r} - \mathbf{R}_k, \mathbf{\Omega}_k) + \Sigma(\mathbf{r}). \tag{3}$$

A. General formalism

For an open system where the charged particles are at a chemical potential μ and at absolute temperature T, the grand partition function is given by

$$Z_G[\gamma,\Sigma] = \sum_{N=0}^{\infty} \frac{1}{N!\,\Lambda^{3N}} \int \prod_{t=1}^{N} d\mathbf{R}_t d\mathbf{\Omega}_t \times \exp\left[-\beta E^{\text{elec}} - \beta E^{\text{ref}} + \sum_{k=1}^{N} \gamma(\mathbf{R}_k, \mathbf{\Omega}_k) \right], \tag{4}$$

where $\beta = 1/(k_B T)$, k_B is the Boltzmann constant, N is the number of particles, R_k is the position of the kth particle, $\mathbf{\Omega}_k$ is its orientation, Λ is the thermal wavelength of a particle, and $\gamma(\mathbf{r},\mathbf{\Omega}) = \beta[\mu - v(\mathbf{r},\mathbf{\Omega})]$, where v an arbitrary applied external field. The integration over the orientation $\mathbf{\Omega}$ of a particle is given explicitly by

$$\int d\mathbf{\Omega} \to \int_0^{\pi} \frac{\sin\theta d\theta}{2} \int_0^{2\pi} \frac{d\varphi}{2\pi} \int_0^{2\pi} \frac{d\psi}{2\pi},$$

where θ, φ, and ψ are the Euler angles that specify the particle orientation.

The quantity E^{elec} represents the energy of electrostatic interaction within the system, and the quantity E^{ref} is the energy of all other types of interactions (e.g., excluded volume interactions and hydration forces). In this work, we focus on particles that only interact with each other through electrostatic forces; consequently, $E^{\text{ref}}=0$.

The electrostatic interaction energy for this system is given by [23,42,43]

$$E^{\text{elec}} = \int d\mathbf{r}d\mathbf{r}'\,\mathcal{Q}(\mathbf{r})G_0(\mathbf{r},\mathbf{r}')\mathcal{Q}(\mathbf{r}) - \sum_k e^{\text{se}}(\mathbf{r}_k,\mathbf{\Omega}_k), \quad (5)$$

where $G_0(\mathbf{r},\mathbf{r}')=\epsilon^{-1}|\mathbf{r}-\mathbf{r}'|^{-1}$ is the Green's function of the Poisson equation, and $e^{\text{se}}(\mathbf{r},\mathbf{\Omega})$ is the self-energy of a particle

$$e^{\text{se}}(\mathbf{R},\mathbf{\Omega}) = \frac{1}{2}\int d\mathbf{r}d\mathbf{r}'\,Q(\mathbf{r}-\mathbf{R},\mathbf{\Omega})G_0(\mathbf{r},\mathbf{r}')Q(\mathbf{r}'-\mathbf{R},\mathbf{\Omega}). \quad (6)$$

Much of the behavior of these systems can be rationalized in terms of a correlation hole [9]—a region of size σ around each counterion, where it is unfavorable for other counterions to be located. At length scales greater than σ, the counterions are weakly correlated, while at shorter length scales, the counterions are strongly correlated but fairly "isolated" [15].

Based on this observation, Weeks and co-workers [20,21] and Santangelo [22] developed approaches that split the interaction between the ions at short and long ranges. The long-range interaction is treated within a mean-field approximation and the short-range interactions with a more precise approach (e.g., computer simulation, liquid state theory, etc.). With an appropriate value for σ, these approaches can successfully describe Monte Carlo results for the full range of electrostatic coupling. However, the value of σ is determined empirically. Additionally, these approaches are not capable of describing systems with dielectric inhomogeneities. In the theory developed in this work, the short-range interactions are treated within a strong-coupling expansion; the long-range interactions are treated with a variational approach, which accounts for fluctuations in the electric potential. Additionally, the value of σ is predicted by the theory in a self-consistent manner.

In order to treat the strong short- and long-range correlations between the charged particles within different approximations, we split the pair interaction between the particles as

$$G_0(\mathbf{r},\mathbf{r}') = G_s(\mathbf{r},\mathbf{r}') + G_l(\mathbf{r},\mathbf{r}'), \quad (7)$$

where $G_s=(1-\mathcal{P})G_0$, $G_l=\mathcal{P}G_0$, and $\mathcal{P}$ is an operator that filters out the short-wavelength contribution to the interactions. The form of the operator $\mathcal{P}$ is fairly arbitrary. In this work, we will explore three different choices

$$\mathcal{P} = \begin{cases} [1-\sigma^2\nabla^2]^{-1}, & \text{Santangelo} \\ e^{\sigma^2\nabla^2}, & \text{Weeks and co-workers} \\ [1-\sigma^2\nabla^2+\sigma^4\nabla^4]^{-1}, & p^4. \end{cases} \quad (8)$$

In these forms for $\mathcal{P}$, the parameter σ denotes the length scale, which separates short-wavelength from long-wavelength phenomena. This parameter can be interpreted as characterizing the size of the correlation hole.

To emphasize the distinction between the short- and long-wavelength contributions to the electrostatic interaction energy of the system, we rewrite Eq. (5) as

$$E^{\text{elec}} = E^{\text{se}} + \frac{1}{2}\int d\mathbf{r}d\mathbf{r}'\,\mathcal{Q}(\mathbf{r})G_l(\mathbf{r},\mathbf{r}')\mathcal{Q}(\mathbf{r}) + \frac{1}{2}\int d\mathbf{r}d\mathbf{r}'\,q(\mathbf{r})G_s(\mathbf{r},\mathbf{r}')q(\mathbf{r}) + \sum_k [u(\mathbf{R}_k,\mathbf{\Omega}_k) - e_s^{\text{se}}(\mathbf{R}_k,\mathbf{\Omega}_k)], \quad (9)$$

where E^{se} is the short-range self-energy of the fixed charges

$$E^{\text{se}} = \frac{1}{2}\int d\mathbf{r}d\mathbf{r}'\,\Sigma(\mathbf{r})G_s(\mathbf{r},\mathbf{r}')\Sigma(\mathbf{r}'), \quad (10)$$

and u is a one-particle interaction potential due to short-wavelength interactions, which is given by

$$u(\mathbf{R},\mathbf{\Omega}) = \int d\mathbf{r}d\mathbf{r}'\,Q(\mathbf{r}-\mathbf{R},\mathbf{\Omega})G_s(\mathbf{r},\mathbf{r}')\Sigma(\mathbf{r}') - e_l^{\text{se}}(\mathbf{R},\mathbf{\Omega}). \quad (11)$$

The self-energy e^{se} of the charged particles has been divided into two separate contributions, e_l^{se} and e_s^{se}, which are given by

$$e_l^{\text{se}}(\mathbf{R},\mathbf{\Omega}) = \frac{1}{2}\int d\mathbf{r}d\mathbf{r}'\,Q(\mathbf{r}-\mathbf{R},\mathbf{\Omega})G_l(\mathbf{r},\mathbf{r}')Q(\mathbf{r}'-\mathbf{R},\mathbf{\Omega}),$$

and

$$e_s^{\text{se}}(\mathbf{R},\mathbf{\Omega}) = \frac{1}{2}\int d\mathbf{r}d\mathbf{r}'\,Q(\mathbf{r}-\mathbf{R},\mathbf{\Omega})G_s(\mathbf{r},\mathbf{r}')Q(\mathbf{r}'-\mathbf{R},\mathbf{\Omega}).$$

Using the Hubbard-Stratonovich transformation [44,45], we convert the expression for the grand partition function [see Eq. (4)] into a functional integral over two fields: ψ_l, which fluctuates over predominately large length scales, and ψ_s, which fluctuates over predominately short length scales. The grand partition function can then be rewritten as

$$Z_G[\gamma,\Sigma] = \frac{e^{-\beta E^{\text{se}}}}{\mathcal{N}_l}\int \mathcal{D}\psi_l(\cdot) \times \exp\left\{-\frac{1}{2\beta}\int d\mathbf{r}d\mathbf{r}'\,\psi_l(\mathbf{r})G_l(\mathbf{r},\mathbf{r}')\psi_l(\mathbf{r}') + \ln \bar{Z}_G^{\text{ref}}[\gamma-\beta u+\beta e_s^{\text{se}}-Qi\psi_l]\right\}, \quad (12)$$

where $\bar{Z}_G^{\mathrm{ref}}$ is a coarse-grained partition function of the reference system, which is given by

$$\bar{Z}_G^{\mathrm{ref}}[\gamma-\beta u+\beta e_s^{\mathrm{se}}-Qi\psi_l]\equiv\langle Z_G^{\mathrm{ref}}[\gamma-\beta u+\beta e_s^{\mathrm{se}}-Qi\psi_l-Qi\psi_s]\rangle_s \tag{13}$$

where the average is defined as

$$\langle(\cdots)\rangle_s\equiv\frac{1}{\mathcal{N}_s}\int\mathcal{D}\psi_s(\cdot)(\cdots)\times\exp\left[-\frac{1}{2\beta}\int d\mathbf{r}d\mathbf{r}'\psi_s(\mathbf{r})G_s^{-1}(\mathbf{r},\mathbf{r}')\psi_s(\mathbf{r}')\right], \tag{14}$$

and the normalization constants are

$$\mathcal{N}_l=\int\mathcal{D}\psi(\cdot)\exp\left[-\frac{1}{2\beta}\int d\mathbf{r}d\mathbf{r}'\psi(\mathbf{r})G_l^{-1}(\mathbf{r},\mathbf{r}')\psi(\mathbf{r}')\right], \tag{15}$$

$$\mathcal{N}_s=\int\mathcal{D}\psi(\cdot)\exp\left[-\frac{1}{2\beta}\int d\mathbf{r}d\mathbf{r}'\psi(\mathbf{r})G_s^{-1}(\mathbf{r},\mathbf{r}')\psi(\mathbf{r}')\right]. \tag{16}$$

The functional Z_G^{ref} is the grand partition function of the reference system (i.e., the system where there are no electrostatic interactions). In this work, the reference system is an ideal gas, which has a grand partition function given by

$$\ln Z_G^{\mathrm{ref}}[\gamma]=\Lambda^{-3}\int d\mathbf{R}d\mathbf{\Omega}e^{\gamma(\mathbf{R},\mathbf{\Omega})}. \tag{17}$$

The expression in Eq. (12) is formally exact; however, in order to perform meaningful calculations, approximations need to be made.

B. Approximation scheme

The strategy here is to treat the long-wavelength interactions within a variational perturbation expansion [46] and the short-range interactions within a strong-coupling expansion [14,15,20–22]. The physical motivation for doing this is based on the important observation that the charges are strongly correlated at short length scales (energy larger k_BT) and only weakly correlated over long length scales.

The functional integration over the short-wavelength modes is performed by using a cumulant expansion

$$\ln\bar{Z}_G^{\mathrm{ref}}[\gamma]\approx\langle\ln Z_G^{\mathrm{ref}}[\gamma-Qi\psi_s]\rangle_s+\frac{1}{2}\langle\ln Z_G^{\mathrm{ref}}[\gamma-Qi\psi_s]\ln Z_G^{\mathrm{ref}}[\gamma-Qi\psi_s]\rangle_s^{(c)}+\cdots, \tag{18}$$

where the superscript (c) denotes a cumulant average. This is equivalent to an expansion in the fugacity of the particles in the system. Using the ideal-gas reference system, this becomes

$$\ln\bar{Z}_G^{\mathrm{ref}}[\gamma]\approx\Lambda^{-3}\int d\mathbf{R}d\mathbf{\Omega}e^{\gamma(\mathbf{R},\mathbf{\Omega})-\beta e_s^{\mathrm{se}}(\mathbf{R},\mathbf{\Omega})}+\cdots, \tag{19}$$

where only the first-order term of the cumulant expansion has been retained.

In order to evaluate the functional integral over the long-wavelength field ψ_l, we use a variational perturbation expansion [43,46,47]. In this method, the fluctuations of the field are assumed to be well approximated by a Gaussian distribution, with a mean value of $\bar{\psi}_l$ and a spatial correlation of $G_{\mathcal{K}}(\mathbf{r},\mathbf{r}')$,

$$H_{\mathcal{K}}[\psi_l]=\frac{1}{2\beta}\int d\mathbf{r}d\mathbf{r}'[\psi_l(\mathbf{r})-\bar{\psi}_l(\mathbf{r})]G_{\mathcal{K}}^{-1}(\mathbf{r},\mathbf{r}')[\psi_l(\mathbf{r}')-\bar{\psi}_l(\mathbf{r}')], \tag{20}$$

where $G_{\mathcal{K}}$ is the renormalized Green's function, which is given by

$$G_{\mathcal{K}}^{-1}(\mathbf{r},\mathbf{r}')=G_l^{-1}(\mathbf{r},\mathbf{r}')+\mathcal{K}(\mathbf{r},\mathbf{r}').$$

Physically, $G_{\mathcal{K}}(\mathbf{r},\mathbf{r}')$ is the renormalized Green's function, which represents how the influence of a charge propagates through the system. The quantity $\mathcal{K}(\mathbf{r},\mathbf{r}')$ is a screening function, and it quantifies how the presence of mobile charges modifies the behavior of the system. This quantity is related to the Debye screening length, as will be discussed below.

Deviations of the field from Gaussian statistics are accounted for by a cumulant expansion. Truncating the variational perturbation expansion at first order, we find

$$\ln Z_G[\gamma,\Sigma]\approx\langle\ln\bar{Z}_G^{\mathrm{ref}}[\gamma-\beta u+\beta e_s^{\mathrm{se}}-Qi\bar{\psi}_l-Qi\delta\psi_l]\rangle_{\mathcal{K}}+\frac{1}{2\beta}\int d\mathbf{r}d\mathbf{r}'i\bar{\psi}_l(\mathbf{r})G_l^{-1}(\mathbf{r},\mathbf{r}')i\bar{\psi}_l(\mathbf{r}')-\int d\mathbf{r}\Sigma(\mathbf{r})i\bar{\psi}_l(\mathbf{r})-\frac{1}{2}\int_0^1 d\zeta\,\mathrm{Tr}\,\mathcal{K}(G_{\zeta\mathcal{K}}-G_{\mathcal{K}})-\frac{\beta}{2}\int d\mathbf{r}d\mathbf{r}'\Sigma(\mathbf{r})G_s(\mathbf{r},\mathbf{r}')\Sigma(\mathbf{r}'), \tag{21}$$

where $G_{\zeta\mathcal{K}}^{-1}=G_l^{-1}+\zeta\mathcal{K}$, and the average $\langle(\cdots)\rangle_{\mathcal{K}}$ is defined as

$$\langle(\cdots)\rangle_{\mathcal{K}}=\frac{1}{\mathcal{N}_{\mathcal{K}}}\int\mathcal{D}\delta\psi(\cdot)(\cdots)\times\exp\left[-\frac{1}{2\beta}\int d\mathbf{r}d\mathbf{r}'\delta\psi(\mathbf{r})G_{\mathcal{K}}^{-1}(\mathbf{r},\mathbf{r}')\delta\psi(\mathbf{r})\right], \tag{22}$$

with the normalization constant $\mathcal{N}_{\mathcal{K}}$ given by

$$\mathcal{N}_{\mathcal{K}}=\int\mathcal{D}\delta\psi(\cdot)\exp\left[-\frac{1}{2\beta}\int d\mathbf{r}d\mathbf{r}'\delta\psi(\mathbf{r})G_{\mathcal{K}}^{-1}(\mathbf{r},\mathbf{r}')\delta\psi(\mathbf{r})\right].$$

For the case where the reference system is an ideal gas, the expression for the coarse-grained partition function of the reference system is given by Eq. (19), and Eq. (21) becomes

$$\ln Z_G[\gamma,\Sigma] \approx \Lambda^{-3}\int d\mathbf{R}d\mathbf{\Omega}\,\exp\Bigg[\gamma(\mathbf{R},\mathbf{\Omega}) - \beta u(\mathbf{R},\mathbf{\Omega}) - \beta e^{\mathrm{se}}_{\mathcal{K}}(\mathbf{R},\mathbf{\Omega}) - \int d\mathbf{r}Q(\mathbf{r}-\mathbf{R},\mathbf{\Omega})i\bar{\psi}_l(\mathbf{r})\Bigg] + \frac{1}{2\beta}\int d\mathbf{r}d\mathbf{r}'\,i\bar{\psi}_l(\mathbf{r})G_l^{-1}(\mathbf{r},\mathbf{r}')i\bar{\psi}_l(\mathbf{r}') - \int d\mathbf{r}\Sigma(\mathbf{r})i\bar{\psi}_l(\mathbf{r}) - \frac{1}{2}\int_0^1 d\zeta\ \mathrm{Tr}\,\mathcal{K}(G_{\zeta\mathcal{K}} - G_{\mathcal{K}}) - \frac{\beta}{2}\int d\mathbf{r}d\mathbf{r}'\Sigma(\mathbf{r})G_s(\mathbf{r},\mathbf{r}')\Sigma(\mathbf{r}'), \tag{23}$$

where

$$e^{\mathrm{se}}_{\mathcal{K}}(\mathbf{R},\mathbf{\Omega}) = \frac{1}{2}\int d\mathbf{r}d\mathbf{r}'Q(\mathbf{R}-\mathbf{r},\mathbf{\Omega})G_{\mathcal{K}}(\mathbf{r},\mathbf{r}')Q(\mathbf{R}-\mathbf{r}',\mathbf{\Omega}). \tag{24}$$

The choice of the quantities $\bar{\psi}_l$ and $\mathcal{K}$ is, in principle, arbitrary. In an exact theory, the physical properties of the system are not dependent on their values. However, the predictions of an approximate theory will, in general, depend on the particular choice of $\bar{\psi}_l$ and $\mathcal{K}$. In the variational approach, the form of these functions is chosen to make the grand partition function stationary with respect to small variations in these functions

$$\frac{\delta \ln Z_G[\gamma,\Sigma]}{\delta i\bar{\psi}_l(\mathbf{r})} = 0, \tag{25}$$

$$\frac{\delta \ln Z_G[\gamma,\Sigma]}{\delta \mathcal{K}(\mathbf{r},\mathbf{r}')} = 0. \tag{26}$$

The first condition [Eq. (25)] leads to a Poisson equation

$$-\frac{1}{4\pi}\nabla^2\phi(\mathbf{r}) = \int d\mathbf{R}d\mathbf{\Omega}Q(\mathbf{r}-\mathbf{R},\mathbf{\Omega})\rho(\mathbf{R},\mathbf{\Omega}) + \Sigma(\mathbf{r}), \tag{27}$$

where $\rho(\mathbf{R},\mathbf{\Omega})$ is the density distribution of the particles, given by

$$\rho(\mathbf{R},\mathbf{\Omega}) = \Lambda^{-3}\exp\Bigg[\gamma(\mathbf{R},\mathbf{\Omega}) - \beta u(\mathbf{R},\mathbf{\Omega}) - \beta e^{\mathrm{se}}_{\mathcal{K}}(\mathbf{R},\mathbf{\Omega}) - \int d\mathbf{r}Q(\mathbf{r}-\mathbf{R},\mathbf{\Omega})i\bar{\psi}_l(\mathbf{r})\Bigg], \tag{28}$$

and $\phi = \beta^{-1}\mathcal{P}^{-1}i\bar{\psi}_l$ is the electric potential. From this, we see that the field $i\bar{\psi}_l$ can be interpreted as the slowly varying portion of the electric potential.

The second condition [Eq. (26)] leads to an expression for the screening function $\mathcal{K}$. In the case where the particles interact only through electrostatic forces [so the reference system is an ideal gas, see Eq. (17)] and where the cumulant expansion for the short-wavelength field [see Eq. (18)] is truncated at first order and the variational perturbation expansion for the long-wavelength field is also truncated at first order, Eq. (26) yields

$$\mathcal{K}(\mathbf{r},\mathbf{r}') = \beta\int d\mathbf{R}d\mathbf{\Omega}Q(\mathbf{r}-\mathbf{R},\mathbf{\Omega})\rho(\mathbf{R},\mathbf{\Omega})Q(\mathbf{r}'-\mathbf{R},\mathbf{\Omega}). \tag{29}$$

The Helmholtz free energy F of the system can be obtained by performing a Legendre transform of the grand partition function [see Eq. (23)], which yields

$$\beta F[\rho,\Sigma] \approx \int d\mathbf{R}d\mathbf{\Omega}\rho(\mathbf{R},\mathbf{\Omega})[\ln\rho(\mathbf{R},\mathbf{\Omega})\Lambda^d - 1] + \frac{1}{2}\int_0^1 d\zeta\ \mathrm{Tr}\,\mathcal{K}(G_{\zeta\mathcal{K}} - G_l) + \frac{1}{2\beta}\int d\mathbf{r}d\mathbf{r}'\,i\bar{\psi}_l(\mathbf{r})G_l^{-1}(\mathbf{r},\mathbf{r}')i\bar{\psi}_l(\mathbf{r}') + \beta\int d\mathbf{r}d\mathbf{r}'Q(\mathbf{r}-\mathbf{R},\mathbf{\Omega})G_s(\mathbf{r},\mathbf{r}')\Sigma(\mathbf{r}') + \frac{\beta}{2}\int d\mathbf{r}d\mathbf{r}'\Sigma(\mathbf{r})G_s(\mathbf{r},\mathbf{r}')\Sigma(\mathbf{r}'). \tag{30}$$

The first term is the ideal-gas contribution to the free energy. The second term is the long-wavelength fluctuation contribution to the electrostatic interaction energy. The third term is a combination of the short-wavelength contribution to the self-energy of the background charge and the short-range interaction energy between the free charges in the system and the background charge.

As with the functions $\bar{\psi}$ and $\mathcal{K}$, the properties of the exact theory should be independent of the choice of the splitting parameter σ. On the other hand, approximate theories do depend on σ. The particular value of σ controls the rate at which the sum of the cumulant (short wavelength) and the variational perturbation (long wavelength) expansions converges to the exact theory. The value of the parameter σ is determined by the condition

$$\frac{\partial F[\rho]}{\partial \sigma} = 0. \tag{31}$$

This approach is similar to the optimized random-phase approximation [48].

The above theory is complete. The main difficulty in evaluating the theory is the determination of the Green's function $G_{\mathcal{K}}$ and the evaluation of the fluctuation integral [the second term in Eq. (30)]. However, in the case of a translationally invariant system, these quantities simplify greatly. We discuss this case below.

C. Translationally invariant systems

Now, we further limit our attention to the situation where the fixed charge distribution $\Sigma(\mathbf{r})$ is a rigid, uniformly distributed, and three-dimensional background charge [i.e., $\Sigma(\mathbf{r}) = \Sigma = -q\rho$] and where the system is translationally invariant [i.e., $\rho(\mathbf{R},\mathbf{\Omega}) = \rho(\mathbf{\Omega})$]. Then, $i\bar{\psi}_l(\mathbf{r}) = 0$, and the

screening function becomes diagonal in Fourier space

$$\hat{\mathcal{K}}(\mathbf{p}) = \beta \int d\mathbf{\Omega} \rho(\mathbf{\Omega}) |\hat{Q}(\mathbf{p},\mathbf{\Omega})|^2, \tag{32}$$

and the one-body potential is given by

$$u(\mathbf{R},\mathbf{\Omega}) = q\hat{G}_s(0)\Sigma - \frac{1}{2}\int_{\mathbf{p}} |\hat{Q}(\mathbf{p},\mathbf{\Omega})|^2 \hat{G}_l(\mathbf{p}). \tag{33}$$

The Helmholtz free energy of the system reduces to

$$\frac{\beta F[\rho]}{V} \approx \int d\mathbf{\Omega} \rho(\mathbf{\Omega})[\ln \rho(\mathbf{\Omega})\Lambda^d - 1] + \frac{1}{2}\int_{\mathbf{p}} \left\{ \ln\left[1 + \frac{\hat{\mathcal{P}}(\mathbf{p})\kappa^2(\mathbf{p})}{p^2}\right] - \frac{\hat{\mathcal{P}}(\mathbf{p})\kappa^2(\mathbf{p})}{p^2} \right\} - \frac{\rho^2 l_B}{2}\hat{G}_s(0), \tag{34}$$

where V is the volume of the system, and $l_B = \beta q^2/\epsilon$ is the Bjerrum length, and $\kappa^2(\mathbf{p}) = 4\pi\hat{\mathcal{K}}(\mathbf{p})$ is a wave-vector-dependent inverse Debye screening length. For the Santangelo and the p^4 splitting operators, $\hat{G}_s(0) = 4\pi\sigma^2$, and $G_l(\mathbf{r},\mathbf{r}) = (\sqrt{3}\sigma)^{-1}$. For the splitting of Weeks and co-workers, $\hat{G}_s(0) = 4\pi\sigma^2$, and $G_l(\mathbf{r},\mathbf{r}) = (\sqrt{\pi}\sigma)^{-1}$.

Equations (32)–(34) form a complete theory for translationally invariant one-component plasmas. In the following sections, we apply this theory to systems of point charges, 8-mer rods of point charges, and line charges.

III. ONE-COMPONENT PLASMA OF POINT CHARGES

In this section, we apply the theory developed in the previous section to the classical one-component plasma, which consists of point charges of magnitude q [i.e., $Q(\mathbf{r}) = q\delta^l(\mathbf{r})$ and $\hat{Q}(\mathbf{p}) = q$] in a uniform neutralizing background charge. There are two key length scales in this system. The first is the Bjerrum length $l_B = \beta q^2/\epsilon$, the distance at which two counterions interact with energy $k_B T$. The other length scale is the mean spacing a between the ions, which for the OCP is given by $a = (4\pi\rho/3)^{-1/3}$, where ρ is the number density of ions in the system. The ratio of these two length scales defines the coupling parameter Γ

$$\Gamma = \frac{l_B}{a} = \left(\frac{4\pi}{3}\rho l_B^3\right)^{1/3}, \tag{35}$$

which characterizes the strength of the electrostatic interactions in the system.

For point charges, the screening length is directly related to the plasma coupling parameter and is given by

$$\kappa^2(\mathbf{p}) = 4\pi\rho l_B = \frac{3}{l_B^2}\Gamma^3. \tag{36}$$

The screening length is independent of the wave vector $\mathbf{p}$, which implies that the particles can screen charge equally well on all length scales.

The Debye-Hückel theory provides the simplest description of the OCP. The Debye-Hückel expression for the electrostatic contribution to the Helmholtz free energy is

$$\frac{\beta F^{\text{elec}}}{V} = -\frac{\kappa^3}{12\pi}, \tag{37}$$

and the corresponding expression for the internal energy is

$$\frac{\beta U}{N} = -\frac{\kappa^3}{8\pi\rho} = -\frac{\sqrt{3}}{2}\Gamma^{3/2}, \tag{38}$$

where N is the number of charged particles in the system.

Combining the expression for the screening length given in Eq. (36) with a choice for the operator $\mathcal{P}$ [e.g., see Eq. (8)], we can compute the free energy of the point-charge OCP by evaluating Eq. (34). With the Santangelo expression for $\mathcal{P}$, we can evaluate the required integrals analytically. In this case, the electrostatic contribution to the Helmholtz free energy F^{elec} [i.e., the sum of the second and third terms in Eq. (34)] is given by

$$\frac{\beta F^{\text{elec}}}{V} = -\frac{\kappa^3}{12\pi}\left[\frac{(1-\kappa\sigma)(1+2\kappa\sigma)^{1/2} - 1 + \frac{3}{2}(\kappa\sigma)^2}{(\kappa\sigma)^3}\right] - \frac{\rho}{2}(\kappa\sigma)^2. \tag{39}$$

The associated expression for the internal energy is

$$\frac{\beta U}{N} = -\frac{\kappa^3}{8\pi\rho}\left[\frac{1-(1+2\kappa\sigma)^{-1/2}}{\kappa\sigma}\right] - \frac{(\kappa\sigma)^2}{2}. \tag{40}$$

If σ is directly set equal to zero, then the Debye-Hückel theory is recovered. This corresponds to neglecting the strong correlations, which occur between the particles at small length scales.

The value of σ needs to be determined by minimizing the free energy. Unfortunately, this cannot be done analytically, but expressions can be obtained for limiting cases. For small values of $\kappa\sigma$, the free energy can be approximated by

$$\frac{\beta F^{\text{elec}}}{V} = -\frac{\kappa^3}{12\pi}\left[1 - \frac{9}{8}(\kappa\sigma) + \frac{3}{2}(\kappa\sigma)^2 + \cdots\right] - \frac{\rho}{2}(\kappa\sigma)^2. \tag{41}$$

By optimizing this expression with respect to the parameter σ, we obtain

$$\sigma = \frac{3}{8}l_B[1 - (3\Gamma)^{3/2} + \cdots]. \tag{42}$$

Therefore, at low values of the plasma coupling parameter (i.e., low ion density), the size of σ is directly related to the Bjerrum length. For large values of $\kappa\sigma$, the free energy can be approximated by

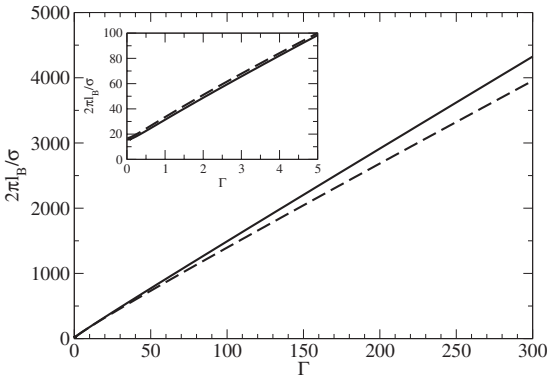

FIG. 1. The splitting parameter as a function of the coupling parameter. The solid line is for the p^4 splitting, and the dashed line is for the Santangelo splitting.

$$\frac{\beta F^{\text{elec}}}{V} = -\frac{\kappa^3}{4\pi}\left[\frac{1}{2}(\kappa\sigma)^{-1} - \frac{\sqrt{2}}{3}(\kappa\sigma)^{-3/2} + \frac{\sqrt{2}}{4}(\kappa\sigma)^{-5/2} + \cdots\right] - \frac{\rho}{2}(\kappa\sigma)^2. \tag{43}$$

In this limit, the parameter σ is given by

$$\frac{2\pi l_B}{\sigma} = 2\pi(6\sqrt{3})^{1/3}\Gamma + \cdots. \tag{44}$$

At high values of the plasma coupling parameter, σ is approximately proportional to the spacing $a = l_B/\Gamma$ between the counterions.

Expressions for the free energy can also be developed with the p^4 and Gaussian forms of the splitting operator [see Eq. (8)]; however, in these cases, the results no longer lead to closed analytical forms and need to be evaluated numerically.

The variation in the splitting parameter σ with the coupling parameter is presented in Fig. 1. The value of σ decreases with the strength of the electrostatic coupling. At small values of the coupling parameter, which corresponds to low ion concentrations, σ becomes proportional to the Bjerrum length l_B. At large values of the coupling parameter, where the ions are in close proximity, σ is nearly linear with the spacing between the ions. This is in agreement with the approaches [10,11] of introducing a high wave-vector cutoff, where the cutoff was found to be inversely proportional to the ion spacing. When the density is fairly low, the counterions interact weakly with each other (the weak-coupling regime). In this case, the size of the correlation hole is related to the Bjerrum length. When the ions are densely packed and forced to be within a distance l_B from each other, they interact very significantly with each other (the strong-coupling regime). In this limit, the size of the correlation hole is related to the mean spacing a between the ions.

In Fig. 2, the variation in the electrostatic interaction energy with the coupling parameter is presented. The symbols are the results of computer simulations. The open circles are the Monte Carlo simulation data from Refs. [49,50]. The solid square are from molecular-dynamics simulations we

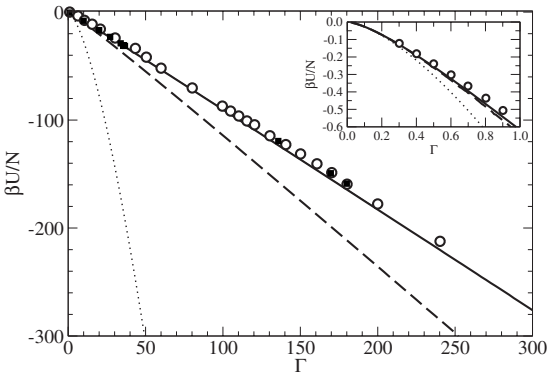

FIG. 2. The internal energy of a OCP of point charges as a function of the coupling parameter: (i) p^4 splitting (solid line), (ii) Santangelo splitting (dashed line), and (iii) Debye-Hückel limiting law (dotted line). The open symbols are Monte Carlo simulation data from Refs. [49,50], and the filled symbols are molecular-dynamics simulation data from the present work.

performed using the GROMACS package [51–54]. The simulations were performed in the *NVT* ensemble with 128 point charges at low values of the coupling parameter ($\Gamma < 100$) and 1024 point charges for higher values of the coupling parameter ($\Gamma > 100$). There is good consistency between our simulation data and Monte Carlo simulation data.

The Debye-Hückel theory given by the dotted line severely overpredicts the strength of the electrostatic interaction, in comparison with the simulation data. The predictions of the theory developed in this work with the Santangelo splitting are given by the dashed line. This represents a substantial improvement over the Debye-Hückel theory; however, it still overestimates the magnitude of the electrostatic interaction energy. The predictions of the theory with the p^4 splitting are given by the solid line, which are in very good agreement with the Monte Carlo simulation data, although they still slightly overestimate the magnitude of the interaction energy. Note that the predictions of the theory with the Weeks' (Gaussian) splitting (not shown) are nearly identical with those of the p^4 splitting.

We find that this theory can describe the internal energy of the system well into the strong-coupling regime for the point-charge OCP model. This approach is similar to the correlation hole corrected Debye-Hückel theory [9] and the Gaussian field theory with a cutoff p_{cut} in p space [10], where the parameter σ is analogous to the size of the correlation hole or $\sim 2\pi/p_{\text{cut}}$. However, the downside of these approaches is the need to include an empirical parameter based on physical grounds such as the correlation hole [9,12] or the high wave-vector cutoff [10,11]. This is not required in our work. One key advantage of this is that the size of the correlation hole can be determined even in situations where it is not clear how σ should depend on the plasma coupling parameter, which occurs when charged particles are no longer point objects.

IV. ONE-COMPONENT PLASMA OF 8-MER RODS

In this section, we examine the influence of the intramolecular structure on the properties of the OCP. We consider a

system of linear 8-mer rods. Each rod consists of $n=8$ point charges, each of magnitude q/n, arranged in a line; adjacent charges are separated by a distance L/n. The number density of the rods is ρ, and the number density of the point charges (monomers) is $n\rho$.

In this case, the charge distribution is given by

$$Q(\mathbf{r},\mathbf{\Omega}) = \frac{q}{n}\sum_{k=1}^{n/2}\{\delta[\mathbf{r} - (2k-1)\hat{\mathbf{n}}(\mathbf{\Omega})L/(2n)] + \delta[\mathbf{r} + (2k-1)\hat{\mathbf{n}}(\mathbf{\Omega})L/(2n)]\}, \quad (45)$$

and the Fourier transform of the charge distribution is given by

$$\hat{Q}(\mathbf{p},\mathbf{\Omega}) = \frac{2q}{n}\sum_{k=1}^{n/2}\cos[(2k-1)\mathbf{p}\cdot\hat{\mathbf{n}}(\mathbf{\Omega})L/(2n)], \quad (46)$$

where $\hat{\mathbf{n}}$ is a unit vector that points parallel to the axis of the rod.

For this system, the three fundamental length scales are the Bjerrum length l_B, the mean distance between the rods a, and the length of the rods L. In addition to the plasma coupling parameter Γ, another important dimensionless quantity is L/l_B, which measures the length of the rods relative to the range of electrostatic interactions in the system. Note that $L/l_B=0$ corresponds to the standard OCP model (i.e., the point-charge limit).

In the context of polyelectrolyte systems, the length scales that are typically used are the Bjerrum length λ_B defined in terms of the charge of the monomers q/n,

$$\lambda_B = \frac{\beta(q/n)^2}{\epsilon} = n^{-2}l_B,$$

the mean distance between the rods a, and the distance $b=L/n$ between the charges on the rods. With these length scales, the key dimensionless parameters are the value of the coupling parameter Γ_0 defined in terms of the monomer density and the monomer Bjerrum length

$$\Gamma_0 = \left(\frac{4\pi}{3}n\rho\lambda_B^3\right)^{1/3}$$

and $b/\lambda_B = nL/l_B$, the spacing between monomers in terms of the monomer Bjerrum length.

For an isotropic system, where $\rho(\mathbf{\Omega})=\rho$, the screening length is given by

$$\kappa^2(\mathbf{p}) = 4\pi\rho l_B\frac{2}{n^2}\sum_{j,k=1}^{n/2}\left[\frac{\sin(j-k)pL/n}{(j-k)pL/n} + \frac{\sin(j+k-1)pL/n}{(j+k-1)pL/n}\right]. \quad (47)$$

Unlike the point-charge system, the screening function for the 8-mer rod system depends on the wave vector. Because the system is isotropic, the screening function depends only on the magnitude of the wave vector. Due to their rigid extended charge distribution, the rods are more effective at screening features at length scales greater than their size than those that are much smaller.

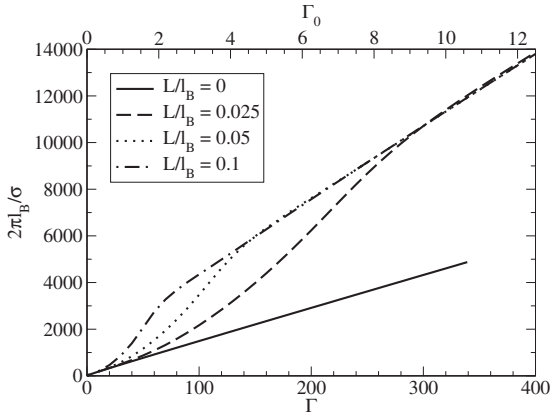

FIG. 3. Variation in the splitting parameter σ with the coupling parameter for 8-mer rods with (i) $L/l_B=0$ (solid line), (ii) $L/l_B=0.025$ (dashed line), and (iii) $L/l_B=0.05$ (dotted line). (iv) $L/l_B=0.1$ (dashed-dotted line).

In this section, we will restrict ourselves to using the p^4 form for the operator $\mathcal{P}$. The variation in the splitting parameter σ with the length of the rod and the plasma parameter is presented in Fig. 3. The case $L/l_B=0$ corresponds to the point-charge system discussed in the previous section; for this system at high values of Γ, the splitting parameter is nearly proportional to the coupling parameter. At low rod densities (i.e., low values of Γ), the variation in σ for all the 8-mer lengths is similar to that for the point-charge model. This is expected, since at these at low densities, the 8-mers are spaced sufficiently far apart that their structure is not important. However, as the density of the particles increases, the structure of the particles becomes important, and the longer particles have a smaller value of σ. That is, the correlation hole is smaller for the longer particles. The value of Γ at which the behavior of the 8-mer rods deviates from that of the point charges depends on the length of the rod: the longer the rod, the sooner the deviation.

At higher values of Γ, the splitting parameter again becomes independent of the length of the particles. This occurs when the distance between the point charges on the 8-mer (i.e., L/n) becomes comparable to the mean distance $a=l_B/\Gamma$ between the 8-mers. In this case, the length of the particles is no longer important in determining the size of the correlation hole. The size of σ is essentially the same as a point-charge model, where the ions have charge q/n and a density equal to $n\rho$, where ρ is the number density of the 8-mer rods in the system. Note, however, this only applies to the size of the correlation hole; the other properties of the system are distinct from the point-charge model as the point charges within each 8-mer are still rigidly bonded and, therefore, strongly correlated.

In order to test the theoretical predictions for the internal energy of the OCP of 8-mer rods, *NVT* molecular-dynamics simulations were performed using the GROMACS package [51–54]. The distance between consecutive point charges was constrained to a fixed distance L/n using the linear constraint solver algorithm [55]. There are no electrostatic interactions between the charges within the rods. The stiffness of the chain is achieved by the use of a harmonic bending potential

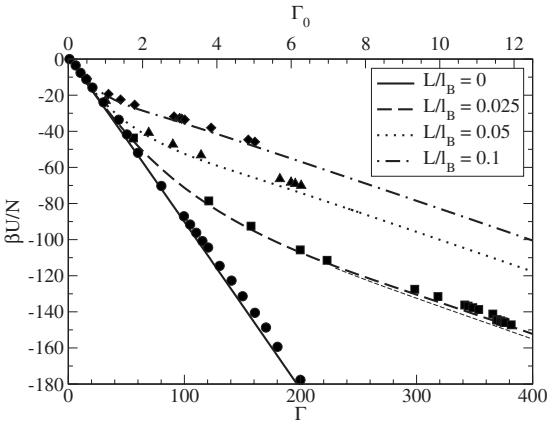

FIG. 4. Variation in the electrostatic interaction energy with the coupling parameter for 8-mer rods with (i) $L/l_B=0$ (solid line, circles), (ii) $L/l_B=0.025$ (dashed line, squares), and (iii) $L/l_B=0.05$ (dotted line, diamonds). (iv) $L/l_B=0.1$ (dashed-dotted line,). The thick lines are the predictions of the present work for the isotropic phase, and the thin lines are the predictions for the nematic phase. The filled symbols are from molecular-dynamics simulations. The thin dashed line represents the energy when the rods are in the nematic phase (see the discussion in Sec. VI).

$$U_{\text{bend}}(\theta) = \frac{K}{2}(\theta - \theta_0)^2, \tag{48}$$

where θ is the angle between two consecutive bonds, $\theta_0=\pi$, and K is the force constant. The value of K is chosen to be sufficiently large to ensure that the 8-mers remained rigid.

In all the simulations, the size of the box was larger than twice the length of the 8-mers. The electrostatic interactions were calculated with the particle-mesh Ewald method [56]. The temperature of the simulations was kept constant using the Nose-Hoover algorithm [57]. The Bjerrum length was varied by adjusting the temperature T of the system.

The electrostatic contribution to the internal energy of 8-mer rods of varying length is given in Fig. 4. The lines are the predictions of the present theory, and the symbols are the results of the molecular-dynamics simulations. The situation where $L/l_B=0$ corresponds to a system of point charges, which was discussed in the previous section. At low values of Γ, where the particle density is low, the energy of the rod systems is the same as that for the point-charge system. This region corresponds to $\Gamma_0<1$, where the mean spacing between the monomers is larger than the monomer Bjerrum length. However, once the rods significantly overlap and the interactions between the monomers become significant (i.e., $\Gamma_0>1$), the energy becomes more positive for the rod systems. As the length of the rod increases, the electrostatic interaction energy of the system becomes less attractive. This is due to the fact that the longer rods are less effective in rearranging themselves in configurations that minimize their mutual repulsive interactions. Overall, the agreement between the theory and the simulation results is quite good; however, in all cases the theory slightly overpredicts the magnitude of the interaction energy.

V. ONE-COMPONENT PLASMA OF CONTINUOUS RODLIKE POLYELECTROLYTES

In this section, we study systems of particles with an infinitely thin uniform line charge of length L and total charge q in a neutralizing uniform background charge. The number density of the rods is ρ. The charge distribution for these particles is given by

$$Q(\mathbf{r},\mathbf{\Omega}) = q\int_{-1/2}^{1/2} ds\,\delta[\mathbf{r} - \hat{\mathbf{n}}(\mathbf{\Omega})L(s-1/2)], \tag{49}$$

where $\hat{\mathbf{n}}$ is a unit vector that points parallel to the axis of the rod, and s denotes the scaled distance along the rod. The corresponding expression for the Fourier transform of the charge distribution is

$$\hat{Q}(\mathbf{p},\mathbf{\Omega}) = q\left[\frac{\sin\,\mathbf{p}\cdot\hat{\mathbf{n}}(\mathbf{\Omega})L/2}{\mathbf{p}\cdot\hat{\mathbf{n}}(\mathbf{\Omega})L/2}\right]. \tag{50}$$

The OCP rod model can be considered as providing a complementary description of polyelectrolyte solutions to the cell model [27–31,33]. In the cell model, the counterions are treated explicitly, and the many-body correlations between the rods are neglected. On the other hand, within the OCP rod model, the counterions are treated simply as a rigid neutralizing background charge, and the many-body rod interactions are treated in detail.

The one-component plasma of line charges was previously studied by Deutsch and Goldenfeld [34,35]. Their approach is similar to an extension of the Debye-Hückel theory to line charges [39–41,43]. This corresponds to setting the splitting parameter $\sigma=0$ in our approach.

For an isotropic system, the screening length is

$$\kappa^2(\mathbf{p}) = 4\pi\rho l_B 2\left[\frac{\mathrm{Si}(pL)}{pL} - \frac{1-\cos(pL)}{(pL)^2}\right], \tag{51}$$

where $\mathrm{Si}(x)=\int_0^x dt\,\sin(t)/t$ is the sine integral. In this case, the screening function and the Green's function $G_{\mathcal{K}}$ depend only on the magnitude of the wave vector $\mathbf{p}$. This reflects the relative inefficiency of the charged rods to screen inhomogeneities in the electric potential, due to their size. Given the expression for the screening length and a choice for the splitting operator, we can make predictions of the properties of the line charge system. In this section, we will restrict ourselves to using the p^4 form for the operator $\mathcal{P}$.

In Fig. 5, we show the variation in the splitting parameter σ with the coupling parameter Γ. The parameter σ represents the size of the "correlation hole." At high values of Γ, when the system is dense with respect to the range of the electrostatic repulsions, the correlation hole is comparable to the mean spacing between the charges. Increasing the length of the rods at a constant value of the coupling parameter decreases the mean spacing between the charges in the system. This is because the charges are more dispersed—spread out over the length of a rod rather than concentrated at a single point. Consequently, we see that the size of the correlation hole decreases as the length of the rods increase. For the longer rods, the size of σ shrinks dramatically with increasing density.

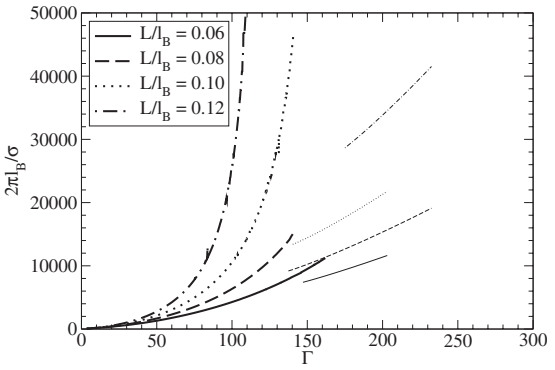

FIG. 5. Variation in the splitting parameter σ with the coupling parameter for rods with (i) L/l_B=0.6 (solid line), (ii) L/l_B=0.8 (dashed line), (iii) L/l_B=1.0 (dotted line), and (iv) L/l_B=1.2 (dashed-dotted line). The thick lines are for the isotropic phase; the thin lines are for the nematic phase.

The variation in the electrostatic interaction energy with the coupling parameter Γ is shown in Fig. 6. The thick lines are for the continuous rods, and the thin lines are for the 8-mer rods. The electrostatic energy for these two systems is similar at low values of the coupling parameter (rod densities); however, they begin to diverge when the spacing between the rods becomes smaller than the spacing L/n between the charges on the 8-mer rods. In this regime, the energy of the continuous rods becomes higher than that for the 8-mer rods, as the 8-mer rods can more easily find configurations that avoid unfavorable interactions with each other.

So far, we have limited our attention to the case where the systems are isotropic. In the next section, we consider the formation of an orientationally ordered nematic phase.

VI. ANALYSIS OF THE NEMATIC PHASE

In the previous sections, we have assumed that the system has remained isotropic and neglected the possibility of orientational ordering of the rods. It has been found that many-body electrostatic interactions always favor [34,35,39–41,43] the alignment of charged rods; however, in the weakly charged regime, the electrostatics cannot overcome the entropic penalty of ordering. It has also been argued that the rods should favor alignment when they are highly charged and favor a nematic transition driven by electrostatics. We examine this effect by using the method developed above to study highly charged rods in a neutralizing background.

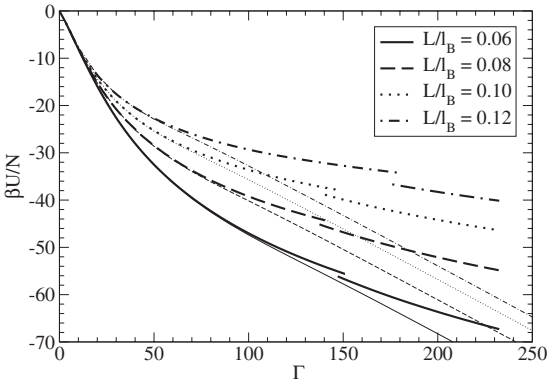

FIG. 6. Electrostatic interaction energy of a one-component plasma of rods as a function of the coupling parameter for rods with (i) L/l_B=0.06 (solid line), (ii) L/l_B=0.08 (dashed line), and (iii) L/l_B=0.10 (dotted line). (iii) L/l_B=0.12 (dashed-dotted line). The thick lines are the for continuous line charges; the thin lines are for 8-mer rods.

To examine the effect of ordering, we introduce the Onsager trial function [58] for the density

$$\rho(\mathbf{\Omega}) = \rho\alpha\frac{\cosh[\alpha\hat{\mathbf{n}}_0\cdot\hat{\mathbf{n}}(\mathbf{\Omega})]}{\sinh(\alpha)}, \tag{52}$$

where the parameter α quantifies the degree of ordering, and $\hat{\mathbf{n}}_0$ is the preferred orientation direction. The limit α=0 corresponds to an isotropic system, and the limit $\alpha\to\infty$ corresponds to a perfectly orientationally ordered system.

Using the Onsager trial function for the density distribution, the ideal contribution to the Helmholtz free energy [i.e., the first term in Eq. (34)] is given by

$$\frac{\beta F^{\mathrm{id}}}{V} = \rho\left[\ln\frac{\alpha\cosh\alpha}{\sinh\alpha} + \frac{\arctan\sinh\alpha}{\sinh\alpha} - 1\right] + \rho[\ln\rho\Lambda^3 - 1]. \tag{53}$$

This term gives an entropic penalty for the orientational ordering of the rods and, consequently, favors the isotropic phase.

With the expression for the distribution of orientations given by Eq. (52), the inverse screening length for the 8-mer rods is

$$\kappa^2(\mathbf{p}) = 4\pi\rho l_B\frac{4}{n^2}\int d\hat{\mathbf{n}}\alpha\frac{\cosh(\alpha\hat{\mathbf{n}}_0\cdot\hat{\mathbf{n}})}{\sinh\alpha} \times\left[\sum_{k=1}^{n/2}\cos((2k-1)\mathbf{p}\cdot\hat{\mathbf{n}}(\mathbf{\Omega})L/(2n))\right]^2, \tag{54}$$

and for the line charges is

$$\kappa^2(\mathbf{p}) = 4\pi\rho l_B\int d\hat{\mathbf{n}}\alpha\frac{\cosh(\alpha\hat{\mathbf{n}}_0\cdot\hat{\mathbf{n}})}{\sinh\alpha}\left[\frac{\sin(\mathbf{p}\cdot\hat{\mathbf{n}}L/2)}{\mathbf{p}\cdot\hat{\mathbf{n}}L/2}\right]^2. \tag{55}$$

An isotropic system corresponds to α=0. In this case, the screening length and therefore the Green's function $G_{\mathcal{K}}$ depend only on the magnitude of the wave vector $\mathbf{p}$. This reflects the fact that the ability of the ordered plasma to screen a given charge distribution depends on its orientation relative to the nematic director.

Given the expression for the screening length of the system, we can compute the Helmholtz free energy of the system by using Eq. (34). The value of the ordering parameter α is determined by minimizing the Helmholtz free energy,

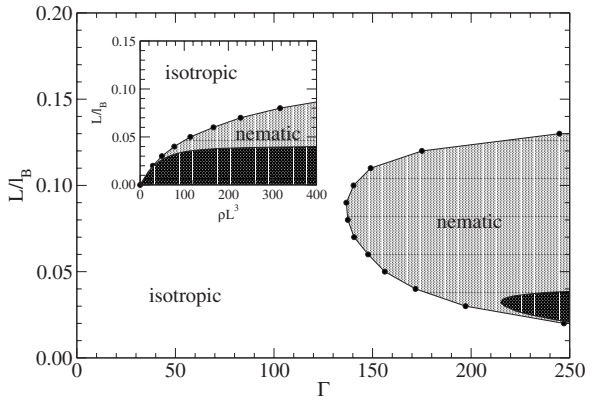

FIG. 7. Phase diagram for a one-component plasma of charged rods. The light shaded region is the nematic phase of the continuous line charges, and the dark shaded region is the nematic phase for the 8-mer rods.

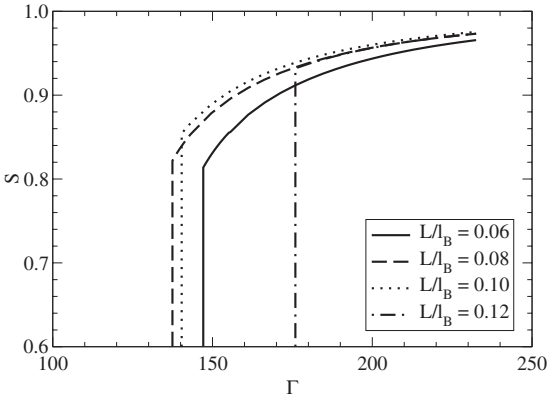

FIG. 8. Variation in the order parameter as a function of coupling parameter for rods with (i) $L/l_B=0.06$ (solid line), (ii) $L/l_B=0.08$ (dashed line), (iii) $L/l_B=0.10$ (dotted line), and (iii) $L/l_B=0.12$ (dashed-dotted line).

$$\frac{\partial \beta F}{\partial \alpha} = 0. \tag{56}$$

If the free energy of the system when it is orientationally ordered (i.e., $\alpha>0$) is lower than when it is isotropic (i.e., $\alpha=0$), then the system will be in the nematic phase. When the opposite is true, it will be in the isotropic phase.

The phase diagram of the OCP rods is presented in Fig. 7. The shaded region represents conditions where the system is nematic, while the unshaded region is where the system is isotropic. The coupling parameter Γ acts as an effective density, and the dimensionless parameter L/l_B acts as an effective temperature. For sufficiently small values of L/l_B (which corresponds to low temperature or strongly charge rods), the length of the rods is too small to drive a nematic transition, and it is expected that the system will be in an isotropic phase. In addition, we expect that for large values of L/l_B, the system should also be entirely in the isotropic phase because the electrostatic coupling is too weak to induce an ordered phase. There should be a closed-loop region, where the nematic phase exists with upper and lower critical points. The electrostatic interactions always favor the formation of the nematic ordering of the rods [39–41,43], so one might expect the existence of an ordered phase at intermediate values of L/l_B. This is indeed the case.

The lightly shaded region denotes the nematic phase for the line charges, while the dark shaded region denotes the nematic phase for the 8-mer rods. The nematic phase is stable over a much larger range of conditions for the line charge system than for the 8-mer system. Therefore, the size of the nematic phase is expected to increase as the number of point charges on an n-mer rod, with the same overall charge and length, increases. The distribution of charge on the rod seems to have a significant influence on the stability of the nematic phase.

In this work, we have been examining a model where there are no excluded volume interactions between the charged rods. To better understand when these interactions will become significant in comparison to the electrostatic interactions, we plot in the inset of Fig. 7 the phase diagram of the charged rods in terms of the variable ρL^3. This variable, unlike the coupling parameter Γ, is independent of the charge on the rods. The larger the charge density of the rods (i.e., the smaller L/l_B), the lower the density of the isotropic-nematic transition.

According to Onsager theory [58,59], for uncharged rods of diameter D and length L, the excluded volume interactions will cause an isotropic to nematic transition at a density

$$\rho L^3 \approx 4.2\frac{L}{D}.$$

Therefore, the relative contribution of the electrostatic and excluded volume interactions is given by the aspect ratio of the rods. For example for rods with an aspect ratio of $L/D=100$, the isotropic-nematic transition (due to excluded volume interactions alone) will occur at $\rho L^3 \approx 420$. For values of $L/l_B<0.07$, the electrostatic interactions between the rods will cause the nematic phase to form at a lower rod density. For example at $L/l_B=0.05$, the electrostatic interactions lead to the formation of a nematic phase at $\rho L^3 \approx 100$. An example of such a system is a rod with an overall charge of $100e_0$ (e_0 is the fundamental unit of charge), where the distance between charges is $b=5\lambda_B$. In this case, the charge density of the rod is sufficiently weak that the counterions will not condense on the surface of the rod, and the counterions can consequently be treated as a uniformly charged background. In water at ambient conditions $\lambda_B \approx 0.7$ nm and, therefore, this would correspond to a rod with length $L=350$ nm (for $L/l_B=0.05$) and diameter $D=3.5$ nm (for $L/D=100$). At these conditions, the electrostatic interactions primarily drive the ordering of the rods rather than the excluded volume interactions. At lower rod charge densities or lower aspect ratios, however, the isotropic-nematic transition will be primarily due to the excluded volume. Therefore, the phase diagram presented in Fig. 7 is only valid for rods with a very large aspect ratio.

The transition from the isotropic to nematic phase is strongly first order. The variation in the order parameter S of an OCP of line charges with the coupling parameter is given in Fig. 8. The order parameter S characterizes the degree of

orientational ordering that is present in a system. A value of 0 corresponds to an isotropic system, and a value of 1 corresponds to a perfectly orientationally aligned system. Within our theory, S is related to the parameter α as

$$S = 1 + \frac{3}{\alpha^2}\left[\frac{1-\alpha(1-e^{-2\alpha})}{1-e^{-2\alpha}}\right].$$

In the nematic phase formed, the rods are highly ordered. This is consistent with the predictions of Deutsch and Goldenfeld [34,35].

In Fig. 5, the thick lines are for systems in the isotropic phase, and the thin lines are for systems in the nematic phase. As the systems change from an isotropic phase to an ordered nematic phase, there is an associated increase in the size of the correlation hole. This can be rationalized in terms of an increase in the mean spacing between the rods. In the nematic phase, the charges on the rods are further from each other, on average, as compared to the isotropic phase. Note that this transition is driven purely by electrostatic interactions, as there are no other interactions in this model. The ordering of the rods is also accompanied by a discontinuous decrease in the electrostatic interaction energy (see Fig. 4 for the 8-mers and Fig. 6 for the line charges). The energy of the nematic phase is lower than the isotropic phase, although the difference is not very large.

A strongly ordered nematic phase was observed in the molecular-dynamics simulations of the 8-mer systems at $L/l_B=0.025$ for coupling parameters $\Gamma>370$. This can be seen in the slight discontinuity of the electrostatic energy of the system shown in Fig. 4. While the change in the order parameter of the system is quite large, the decrease in the energy of the system across the isotropic-nematic transition is fairly small; this is in agreement with the theory. However, the transition occurs at a much higher value of Γ than predicted by the theory. This may be due to the fact that there is only a slight free-energy difference between the nematic and isotropic phases. Consequently, while the theory is capable of computing the absolute properties of the rod systems rather accurately, the free-energy difference between the two phases may be too subtle for the theory to precisely predict the transition.

VII. CONCLUSIONS

In this work, we have developed an approximate theory to describe the properties of mobile particles with extended charge densities in the presence of a background charge. By dividing the fluctuations of the electric potential into short-wavelength and long-wavelength contributions and treating each of these within an appropriate approximation scheme, this theory is able to provide quantitative predictions for the properties of these systems from the weak- to the strong-coupling regimes.

We apply this theory to investigate the properties of a one-component plasma composed of point charges, 8-mer rods of point charges, and continuous line charges. In each of these systems, the theory is able to provide quantitatively accurate predictions for the electrostatic interaction energy, with respect to molecular-dynamics simulation data. However, the theory slightly overpredicts the magnitude of the interaction.

For the rod systems, a nematic phase is present over a window of rod lengths L/l_B. The formation of this phase is driven entirely by electrostatic interactions. If the rod length is too small, then the rods are too short to order. If the rods are too long, then the charge density is too weak for the electrostatic interactions to order the rods. The nematic phase is much more stable for the continuous line charges than for the 8-mer rods. Therefore, we find that the phase behavior of linear polyelectrolytes is sensitive to their charge distribution.

In future, we intend to extend this work beyond the one-component plasma model to include polyelectrolyte systems with mobile counterions. Unlike for the one-component plasma model, excluded volume interactions cannot be neglected for this system, as these are required to counter the detrimental collapse of the counterions onto the polyelectrolytes. In order to properly represent this short-wavelength feature of the system within the present theory, the cumulant expansion for the functional integral over the short-wavelength interaction field ψ_s must be evaluated to at least second order. It is only at this level of approximation that the balance between the attractive electrostatic interactions and the repulsive excluded volume interactions between the counterions and the polyelectrolytes can be captured. Work along these lines is currently under way.

ACKNOWLEDGMENTS

M.M.H. acknowledges support from an EC Marie Curie Action (Grant No. MEST-CT-2004-503750). A Karatrantos acknowledges support from an EC Marie Curie Action (Grant No. MEST-CT-2005-020826).

[1] M. Baus, Phys. Rep. **59**, 1 (1980).
[2] S. Ichimaru, H. Iyetomi, and S. Tanaka, Phys. Rep. **149**, 91 (1987).
[3] M. J. Gillan, J. Phys. C **7**, L1 (1974).
[4] R. G. Palmer, J. Chem. Phys. **73**, 2009 (1980).
[5] J. F. Springer, M. A. Pokrant, and F. A. Stevens, Jr., J. Chem. Phys. **58**, 4863 (1973).
[6] K.-C. Ng, J. Chem. Phys. **61**, 2680 (1974).
[7] F. Lado, S. M. Foiles, and N. W. Ashcroft, Phys. Rev. A **28**, 2374 (1983).
[8] F. J. Rogers and D. A. Young, Phys. Rev. A **30**, 999 (1984).
[9] S. Nordholm, Chem. Phys. Lett. **105**, 302 (1984).
[10] N. V. Brilliantov, Contrib. Plasma Phys. **38**, 489 (1998).
[11] A. G. Moreira and R. R. Netz, Eur. Phys. J. D **8**, 145 (2000).
[12] M. C. Barbosa, M. Deserno, and C. Holm, Europhys. Lett. **52**, 80 (2000).

[13] M. Stevens, Biophys. J. **80**, 130 (2001).
[14] B. I. Shklovskii, Phys. Rev. E **60**, 5802 (1999).
[15] A. G. Moreira and R. R. Netz, Phys. Rev. Lett. **87**, 078301 (2001).
[16] C. W. Outhwaite, L. B. Bhuiyan, and S. Levine, J. Chem. Soc., Faraday Trans. 2 **76**, 1388 (1980).
[17] C. Outhwaite and L. B. Bhuiyan, J. Chem. Soc., Faraday Trans. 2 **78**, 775 (1982).
[18] C. W. Outhwaite and L. B. Bhuiyan, J. Chem. Soc., Faraday Trans. 2 **79**, 707 (1983).
[19] Y. Burak, D. Andelman, and H. Orland, Phys. Rev. E **70**, 016102 (2004).
[20] Y.-G. Chen, C. Kaur, and J. Weeks, J. Phys. Chem. B **108**, 19874 (2004).
[21] Y.-G. Chen and J. D. Weeks, Proc. Natl. Acad. Sci. U.S.A. **103**, 7560 (2006).
[22] C. D. Santangelo, Phys. Rev. E **73**, 041512 (2006).
[23] M. M. Hatlo and L. Lue, Soft Matter **5**, 125 (2009).
[24] J. L. Barrat and J. F. Joanny, Adv. Chem. Phys. **94**, 1 (1996).
[25] C. Holm, J. F. Joanny, K. Kremer, R. R. Netz, P. Reineker, C. Seidel, T. A. Vilgis, and R. G. Winkler, Adv. Polym. Sci. **166**, 67 (2004).
[26] A. Yethiraj, J. Phys. Chem. B **113**, 1539 (2009).
[27] A. Katchalsky, Pure Appl. Chem. **26**, 327 (1971).
[28] L. Guldbrand, Mol. Phys. **67**, 217 (1989).
[29] L. Nilsson, L. Guldbrand, and L. Nordenskiold, Mol. Phys. **72**, 177 (1991).
[30] N. Gronbech-Jensen, R. J. Mashl, R. F. Bruinsma, and W. M. Gelbart, Phys. Rev. Lett. **78**, 2477 (1997).
[31] A. P. Lyubartsev, J. X. Tang, P. A. Janmey, and L. Nordenskiold, Phys. Rev. Lett. **81**, 5465 (1998).
[32] M. Deserno, C. Holm, and S. May, Macromolecules **33**, 199 (2000).
[33] M. Deserno and C. Holm, Mol. Phys. **100**, 2941 (2002).
[34] J. M. Deutsch and N. D. Goldenfeld, J. Phys. A **15**, L71 (1982).
[35] J. M. Deutsch and N. D. Goldenfeld, J. Phys. (Paris) **43**, 651 (1982).
[36] C. Y. Shew and A. Yethiraj, J. Chem. Phys. **106**, 5706 (1997).
[37] T. Hofmann, R. G. Winkler, and P. Reineker, J. Chem. Phys. **114**, 10181 (2001).
[38] G. A. Carri and M. Muthukumar, J. Chem. Phys. **111**, 1765 (1999).
[39] I. I. Potemkin, R. E. Limberger, A. N. Kudlay, and A. R. Khokhlov, Phys. Rev. E **66**, 011802 (2002).
[40] I. I. Potemkin and A. R. Khokhlov, J. Chem. Phys. **120**, 10848 (2004).
[41] I. I. Potemkin, N. N. Oskolkov, A. R. Khokhlov, and P. Reineker, Phys. Rev. E **72**, 021804 (2005).
[42] J. D. Jackson, *Classical Electrodynamics* (Wiley, New York, 1975).
[43] L. Lue, Fluid Phase Equilib. **241**, 236 (2006).
[44] R. L. Stratonovich, Dokl. Akad. Nauk SSSR **115**, 1097 (1957).
[45] J. Hubbard, Phys. Rev. Lett. **3**, 77 (1959).
[46] R. A. Curtis and L. Lue, J. Chem. Phys. **123**, 174702 (2005).
[47] H. Kleinert, *Path Integrals in Quantum Mechanics, Statistics, and Polymer Physics*, 2nd ed. (World Scientific, Singapore, 1995).
[48] H. C. Andersen and D. Chandler, J. Chem. Phys. **57**, 1918 (1972).
[49] S. G. Brush, H. L. Sahlin, and E. Teller, J. Chem. Phys. **45**, 2102 (1966).
[50] W. L. Slattery, G. D. Doolen, and H. E. DeWitt, Phys. Rev. A **26**, 2255 (1982).
[51] H. Bekker, H. Berendsen, E. J. Dijkstra, S. Achterop, R. van Drunen, D. van der Spoel, A. Sijbers, H. Keegstra, B. Reitsma, and M. K. R. Renardus, GROMACS: A Parallel Computer for Molecular Dynamics Simulation, in *Physics Computing*, edited by R. A. de Groot, and J. Nadrchal (World Scientific, Singapore, 1993), p. 252–256.
[52] H. J. C. Berendsen, D. van der Spoel, and R. van Drunen, Comput. Phys. Commun. **91**, 43 (1995).
[53] E. Lindahl, B. Hess, and D. van der Spoel, J. Mol. Model. **7**, 306 (2001).
[54] D. van der Spoel, E. Lindahl, B. Hess, G. Groenhof, A. Mark, and H. J. C. Berendsen, J. Comput. Chem. **26**, 1701 (2005).
[55] B. Hess, H. Bekker, H. Berendsen, and J. Fraaije, J. Comput. Chem. **18**, 1463 (1997).
[56] T. Darden, D. York, and L. Pedersen, J. Chem. Phys. **98**, 10089 (1993).
[57] S. Nose, Mol. Phys. **52**, 255 (1984).
[58] L. Onsager, Ann. N.Y. Acad. Sci. **51**, 627 (1949).
[59] P. G. de Gennes and J. Prost, *The Physics of Liquid Crystals*, 2nd ed. (Oxford University, Oxford, 1993).